Yan Zhou, Rajesh Ramaneti, Julian Anaya, Svetlana Korneychuk, Joff Derluyn, Huarui Sun [iD], James Pomeroy [iD], Johan Verbeeck, Ken Haenen [iD], and Martin Kuball

View Online   Export Citation   CrossMark

ARTICLES YOU MAY BE INTERESTED IN

Thermal characterization of polycrystalline diamond thin film heat spreaders grown on GaN HEMTs

Yan Zhou,[1,a] Rajesh Ramaneti,[2,3] Julian Anaya,[1] Svetlana Korneychuk,[4] Joff Derluyn,[5] Huarui Sun,[1] James Pomeroy,[1] Johan Verbeeck,[4] Ken Haenen,[2,3] and Martin Kuball[1]

[1]Center for Device Thermography and Reliability (CDTR), H. H. Wills Physics Laboratory, University of Bristol, Tyndall Avenue, Bristol BS8 1TL, United Kingdom
[2]Institute for Materials Research (IMO), Hasselt University, Wetenschapspark 1, 3590 Diepenbeek, Belgium
[3]IMOMEC, IMEC vzw, Wetenschapspark 1, 3590 Diepenbeek, Belgium
[4]Electron Microscopy for Material Science (EMAT), University of Antwerp, Groenenborgerlaan 171, 2020 Antwerp, Belgium
[5]EpiGaN NV, Kempische Steenweg 293, 3500 Hasselt, Belgium

Polycrystalline diamond (PCD) was grown onto high-k dielectric passivated AlGaN/GaN-on-Si high electron mobility transistor (HEMT) structures, with film thicknesses ranging from 155 to 1000 nm. Transient thermoreflectance results were combined with device thermal simulations to investigate the heat spreading benefit of the diamond layer. The observed thermal conductivity (κ_{Dia}) of PCD films is one-to-two orders of magnitude lower than that of bulk PCD and exhibits a strong layer thickness dependence, which is attributed to the grain size evolution. The films exhibit a weak temperature dependence of κ_{Dia} in the measured 25–225 °C range. Device simulation using the experimental κ_{Dia} and thermal boundary resistance values predicts at best a 15% reduction in peak temperature when the source-drain opening of a passivated AlGaN/GaN-on-Si HEMT is overgrown with PCD. Published by AIP Publishing. [http://dx.doi.org/10.1063/1.4995407]

Gallium nitride (GaN) has attracted major attention for electronic and optoelectronic device applications[1] due to its wide bandgap of 3.4 eV, very high breakdown voltage (3×10^6 V/cm), and high peak (3×10^7 cm/s) and saturation (1.5×10^7 cm/s) electron velocities.[2] However, the high operating power density of AlGaN/GaN high electron mobility transistors (HEMTs), combined with localized near-junction self-heating, can cause a large temperature rise which must be minimized to avoid premature degradation.[3–5] Heat transport in the near-junction region of GaN HEMTs is particularly important and is influenced by the thermal conductivities of GaN, strain relief, and substrate layers; the effective thermal boundary resistance (TBR_{eff}) between the epilayers and substrate can also be a significant contribution.[6,7] The heat extraction benefit of integrating high thermal conductivity diamond with GaN-based devices has recently been demonstrated, resulting in improved thermal management.[8] Bulk polycrystalline diamond (PCD) grown by chemical vapor deposition can reach thermal conductivities almost as high as those of single-crystal diamond,[9] but has the advantage of larger wafer-size availability which is suitable for commercial semiconductor manufacturing. To maximize the benefit of diamond heat spreaders integrated with AlGaN/GaN HEMTs, PCD should be placed as close as possible to the Joule heating location, which is the 2DEG channel at the AlGaN/GaN interface, close to gate foot on the drain side. PCD heat spreaders can be integrated in different areas of an AlGaN/GaN HEMT, including (a) replacing the Si or SiC substrate by direct growth[10] or wafer bonding,[11] and (b) growing PCD directly on top of the passivated HEMT channel.[12,13] For the first strategy, both the

electrical[10,14] and thermal device characterizations[15–18] have been studied extensively, with a potential threefold increase in output power density reported.[15,17] For the second strategy, improved electrical performance and 20% lower device temperature have been shown for PCD-capped and gate-after-PCD HEMT devices.[19–21] However, the thermal resistance of PCD-on-HEMT structures has not been measured directly in previous studies.[19–21]

In this work, we use transient thermoreflectance (TTR) systematically to evaluate the thermal properties of PCD film heat spreaders fabricated on the Si_3N_4 passivation layer of typical AlGaN/GaN-on-Si HEMT structures (diamond-on-GaN HEMTs), using diamond film thicknesses ranging from 155 to 1000 nm. The thermal properties of these samples were characterized over the temperature range from 25 to 225 °C. This information was then used in a finite-element model of a multi-finger AlGaN/GaN-on-Si HEMT device to evaluate the heat spreading benefit of integrating PCD in close proximity to the channel.

The AlGaN/GaN heterostructure studied here was grown by metal-organic chemical vapor deposition (MOCVD) on a Si(111) substrate, consisting of 20 nm-thick AlGaN on a 600 nm-thick GaN buffer layer and a strain-relief-layer [Fig. 1(a)]. The AlGaN/GaN heterostructure was passivated using a 50 nm-thick layer of amorphous stoichiometric Si_3N_4, grown in-situ using MOCVD. After cleaning and a low-power (20 W) O_2-plasma treatment of the Si_3N_4 surface to ensure a uniform seeding of diamond nanoparticles,[22] the seeded-passivated heterostructure substrate was then loaded onto a microwave-CVD reactor for the PCD growth at 650 °C, 20 Torr and a CH_4/H_2 gas flow of 485/15 sccm.[23] PCD layers were grown on a number of samples under the same step-by-step conditions to yield a thickness ranging from 155 to

a)Author to whom correspondence should be addressed: yan.zhou@bristol.ac.uk
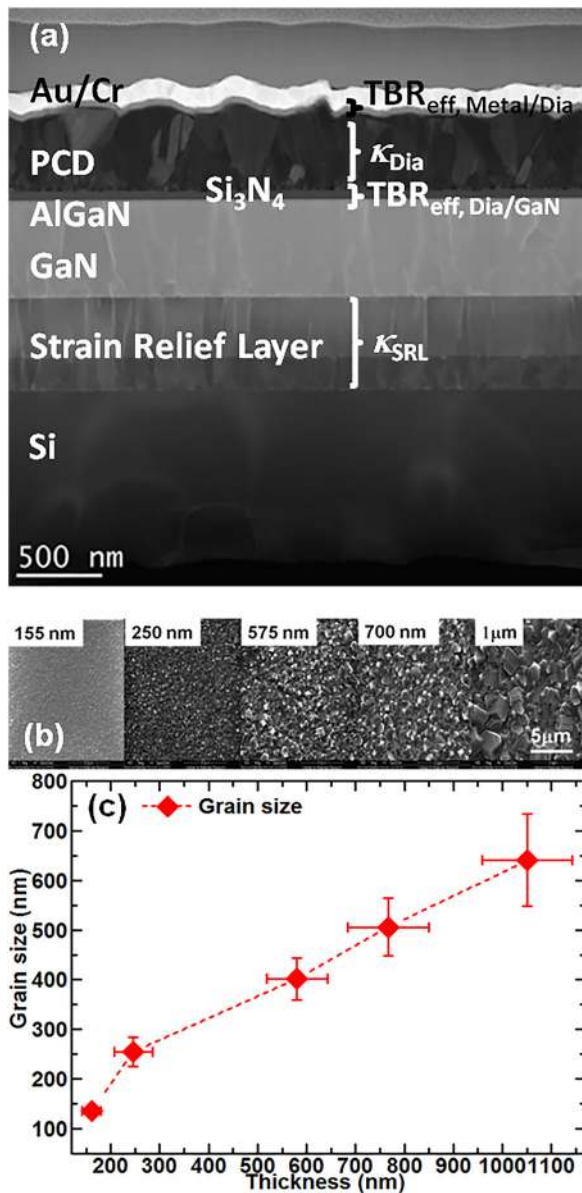
FIG. 1. (a) Cross-sectional TEM image of the measured structure. (b) SEM micrographs on the diamond film surfaces with film thickness labeled. (c) In-plane grain size at the diamond surface as a function of the PCD film thickness.

1000 nm, followed by surface oxidation in H_2SO_4-KNO_3 solution to remove graphitic phases. A 30 nm-thick Cr adhesion layer and a 100 nm-thick Au film were then deposited onto the diamond as a transducer for the thermoreflectance measurements. Figure 1(a) shows the cross-sectional Transmission Electron Microscopy (TEM) image of the heterostructure after completion of the processing. Sharp interfaces and no damage underlying device heterostructure are observed, even after the diamond growth. Figure 1(a) also illustrates the columnar outgrowth of diamond into micrograins.

Figure 1(b) shows the surface morphology of the PCD films imaged by Scanning Electron Microscopy (SEM). The in-plane grain size on the top surface was determined using the three-circle procedure,[24] with the results displayed in Fig. 1(c). The observed in-plane grain size demonstrates an approximately linear correlation with the diamond film thickness. The thermoreflectance measurements were carried

out using a 355 nm frequency-tripled Nd:YAG pump laser with a pulse duration of 8 ns and a spot size of 70 μm as a heating pulse to induce a rapid temperature rise at the surface of gold. A 532 nm continuous wave (CW) laser (frequency-doubled Nd:YAG) with a spot size of $\sim$2 μm was used to probe the reflectivity change, which is directly proportional to the temperature rise at the gold surface. More details of this technique are described in Refs. 16, 17, and 25. The temperature dependent analysis of these samples was carried out by heating the substrates from 25 to 225 °C using a Linkam TS600 microscope chamber.

Figure 2(a) shows the normalized thermoreflectance transients of diamond-on-GaN HEMT structures, measured at 25 °C for a range of PCD film thicknesses. The thermoreflectance data was analyzed by solving the transient heat equation analytically for the multilayer material stack using the transmission-line axis-symmetric model described by Hui *et al.*,[26,27] which has been proved to be able to deal with complex multilayer samples accurately.[26,27] The inputs of this model are the thermal conductivity, thickness, density, and volumetric heat capacity of each layer/material, as well as the geometrical and temporal characteristics of both pump and probe lasers. A reference TTR measurement was made first on each GaN-on-Si wafer prior to diamond growth, using an identical transducer; an example plot is shown in Fig. 2(a). The parameters obtained for the GaN-on-Si HEMT structure are consistent with values reported in Refs. 28 and 29. Measured strain-relief-layer thermal conductivities (κ_{SRL}) were found to be sample-dependent and within the 4.3–9 W/mK range, consistent with previous reports.[30–32] Table I shows the resulting parameters which were fixed in the subsequent simulations. The remaining parameters, i.e., the TBR_{eff} between the metal transducer and diamond ($TBR_{eff, Metal/Dia}$), the thermal conductivity of diamond (κ_{Dia}), and the TBR_{eff} between diamond and GaN ($TBR_{eff, Dia/GaN}$), are treated as variables and adjusted to fit the experimental data. It should be noted that the measured κ_{Dia} value represents a depth average in the cross-plane direction (through the layer). For simplification, the thin Cr layer was

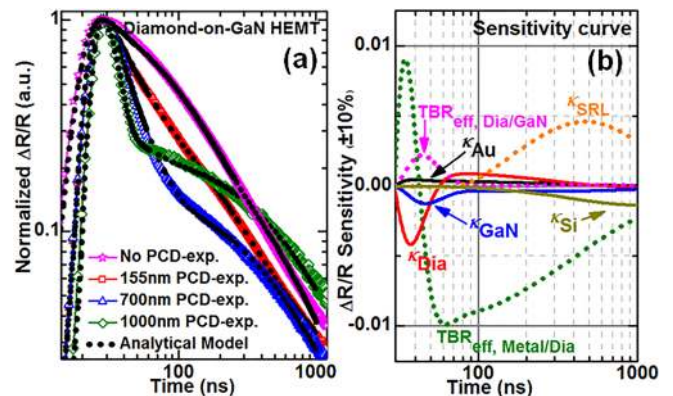FIG. 2. (a) Normalized thermoreflectance transients of the GaN-on-Si reference sample and of diamond-on-GaN HEMT samples for diamond thicknesses of 155 nm, 700 nm, and 1000 nm, on a logarithmic scale; lines represent experimental values, and dots represent the analytical model fitted. (b) Sensitivity analysis, with the sensitivity of △R/R corresponding to ±10% change in each input parameter in the model.

TABLE I. Fixed input parameters for analytical model simulation.

Layer	Au	Diamond	GaN	Si
Thickness (nm)	100	155–1000	600	500 000
Thermal conductivity $(W\,m^{-1}\,K^{-1})$	200[a]	Fitted	124[b]	148[c]
Specific heat $(J\,kg^{-1}\,K^{-1})$	129[d]	500[e]	430[f]	665.2[g]
Density $(kg\,m^{-3})$	19 800	3510	6150	2320

[a]Consistent with Refs. 31 and 34.
[b]Reference 28.
[c]Reference 29.
[d]Reference 35.
[e]References 36 and 37.
[f]Reference 38.
[g]Reference 39.

lumped into a single thermal boundary resistance between Au and diamond, $TBR_{eff,\ Metal/Dia}$. Similarly, the thin AlGaN barrier layer and Si_3N_4 layer were lumped into $TBR_{eff,\ Dia/GaN}$. Given the nonlinear nature of the problem, the variables were determined via a nonlinear fitting routine using a Monte-Carlo algorithm to populate the space of initial values of $TBR_{eff,\ Metal/Dia}$, κ_{Dia}, and $TBR_{eff,\ Dia/GaN}$. The initial values of these variables, together with the fixed parameters, were then used in a Nelder-Mead algorithm in order to achieve the best fit (and fitting uncertainty) to the experimental data, similar to the method described in Ref. 33. Figure 2(a) shows an example of the experimental and analytical model curves.

Figure 2(b) illustrates the sensitivity plot for each parameter in the heat diffusion model. Some parameters have distinct time constants, whereas others overlap, e.g., $TBR_{eff,\ Dia/GaN}$ mostly impacts the measured response in the 10–40 ns time window, while the diamond thermal conductivity (κ_{Dia}) mainly affects the 0–40 ns range. Considering this, a 99% confidence level was set in the Monte-Carlo model to obtain the best fitting range for each parameter. The conservative gold layer thickness variation due to the diamond surface roughness is ~80–120 nm, as measured by TEM. To account for this range, fitting was performed with the transducer thickness fixed at the maximum and minimum values to estimate the uncertainty introduced to the remaining fitting parameters.

Figure 3(a) summarizes the above analysis, showing that κ_{Dia} increases almost linearly with the PCD thickness. To

fundamentally understand this PCD thermal conductivity behavior, the evolution of the in-plane grain size with films thickness needs to be considered. As the in-plane grain size clearly correlates with the diamond film thickness (see Fig. 1), this increases κ_{Dia} for thicker layers due to the increased phonon mean-free-path.[40,41] We note that κ_{Dia} (from 55 ± 15 to 320 ± 150 W/mK) is one-to-two orders of magnitude lower than that of single-crystal diamond, consistent with the thickness-dependency concluded in the literature.[42] An incremental layer-by-layer (considering that the grain size varies with the depth through the diamond layer) Callaway-like KC-model[40] was fitted to the diamond thermal conductivities determined here. A good agreement is observed between the measurement and model in the diamond thickness range of 0–800 nm, using an intra-grain thermal conductivity ($\kappa_{lattice}$) of 1250 W/mK[40,43] and a grain boundary thermal conductance (G) of 0.3 GW/m^2 K. The modeled and measured values diverge above a diamond thickness of 800 nm, suggesting that either $\kappa_{lattice}$ or G is not constant through the diamond film.

The PCD grain size in thin layers is much shorter than the phonon mean-free-path in single-crystal diamond, which essentially limits heat transport. Grain boundaries are prone to accumulate defects, including disordered-bonding structures, which lower the G value. We also note that $TBR_{eff,\ Dia/GaN}$ is higher than that in recent reports,[15–17,44,45] mainly attributed to the thicker Si_3N_4 in our structure (which is very commonly used for passivation and also as a protective layer during the initial diamond growth), and is not identical in all samples although the growth parameters were nominally identical [see Fig. 3(b)]; this variation may be related to the slightly inhomogeneous initial seeding conditions or different initial microstructual disorders.[46,47] Figure 3(c) shows κ_{Dia} as a function of temperature. All samples exhibit a negligible temperature dependence. This is very different from bulk PCD where it is seen to decrease with temperature[9] but similar to the characteristics of the disordered material.[48] Figure 3(d) shows the high-resolution TEM image in the vicinity of a diamond grain boundary, where numerous disordered intragrain structures such as twins and stacking faults are observed, which will greatly increase the phonon scattering within the diamond grains. Thus, the diamond crystallinity (the ordering of the sp^3 phase within the
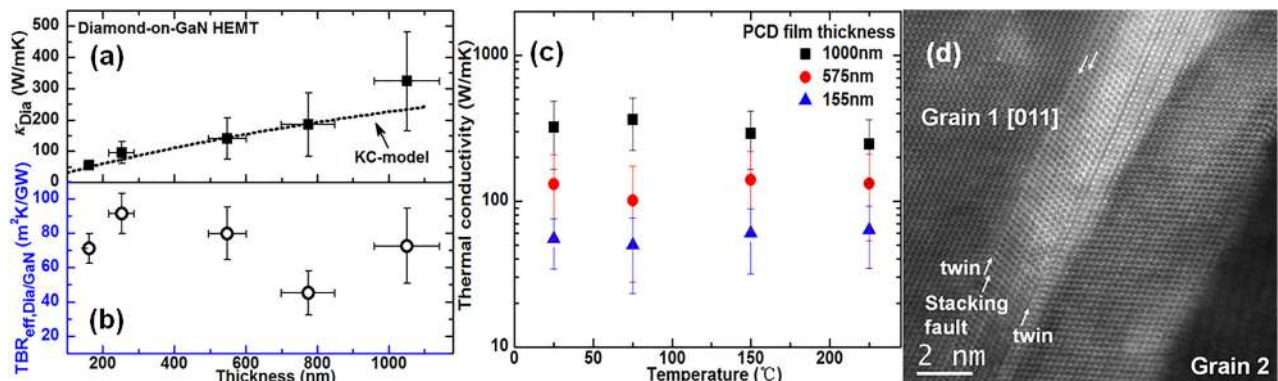

FIG. 3. (a) Thermal conductivity of PCD and (b) TBR between PCD and GaN as a function of the PCD film thickness. The line is a predicted KC-model.[40] (c) Thermal conductivity of PCD films from 25 to 225 °C measured by transient thermoreflectance. (d) High resolution ADF-STEM (annular dark-field scanning transmission electron microscopy) image of the diamond intragrain structure.

diamond grain), amorphicity, and defects[49] can also introduce significant phonon scattering, lowering $\kappa_{lattice}$ and κ_{Dia}.

To investigate the impact of PCD heat spreaders on the actual thermal characteristics of devices, a finite-element steady-state thermal model of a $16 \times 125\,\mu m$-wide, $50\,\mu m$ gate-pitch AlGaN/GaN-on-Si HEMT was constructed in ANSYS based on a layer structure shown in Fig. 1(a),[42] using the experimentally determined κ_{Dia} and TBR_{eff} values. The power density was set at a typical value of 5 W/mm, dissipated in a $0.5\,\mu m$-long, 100 nm-thick volume at the drain edge of the gate foot where most Joule heating occurs.[50] Given that the cross-plane thermal conductivity is always higher than the in-plane thermal conductivity for this columnar PCD,[51] the experimental value can thus be used to determine an upper limit of the expected thermal benefit of PCD. By adding a PCD heat spreader on top of the device source-drain opening, Fig. 4(a) shows that a 12% maximum reduction in peak channel temperature could be achieved using a 1000 nm PCD film. We note that if the TBR_{eff} at the diamond/GaN interface is not included, then there is a further 10% temperature reduction. As the thermal conductivity varies through the diamond films in the cross-plane direction, we have also investigated the effect of this on the device thermal properties by simulating the 1000 nm PCD film using from one to five layers, corresponding to the thermal conductivity data of each layer extracted from Fig. 3(a).

Figure 4(a) shows that there is little difference in peak channel temperature by considering the gradient in thermal conductivity, illustrating the validity and simplicity of using the average κ_{Dia} to simulate the steady-state thermal performance of devices. The device peak temperature as a function of the PCD film thickness, when only covering the source-drain opening, is illustrated in Fig. 4(b). Little further thermal benefit is predicted when using PCD films thicker than $2\,\mu m$, with only a maximum 15% reduction, using either the measured cross-plane κ_{Dia} or using the 0.4–0.6 anisotropic thermal conductivity ratio from the literature.[42] These results highlight the importance of the crystalline quality of the very first micrometer of diamond in heat spreading layers. However, if PCD could be grown on both source-drain opening and metal contacts [Fig. 4(b) inset], a $1.5\times$ better thermal benefit would be achieved for thicker films by increasing the area of the heat spreader.

PCD heat spreader structures were grown on passivated AlGaN/GaN HEMT structures and studied, with diamond film thicknesses varying from 155 to 1000 nm. The results show that κ_{Dia} has a strong film thickness dependence, which can be attributed to the in-plane grain size evolution with the film thickness, with the measured values of 320 ± 150 W/mK for $1\,\mu m$-thick PCD, which is nearly one order of magnitude lower than the bulk PCD value of ~2200 W/mK. The PCD layers do not show a sizable temperature dependence of κ_{Dia} in the measured range from 25 to 225 °C. Transistor thermal modeling shows that growing the PCD film heat spreader in the source-drain opening only reduces the peak temperature by a maximum of 15%. There is limited thermal benefit when the PCD film thickness is increased beyond $\sim2\,\mu m$, unless both source-drain opening and metal contacts are overgrown by PCD to increase the area of the heat spreader.
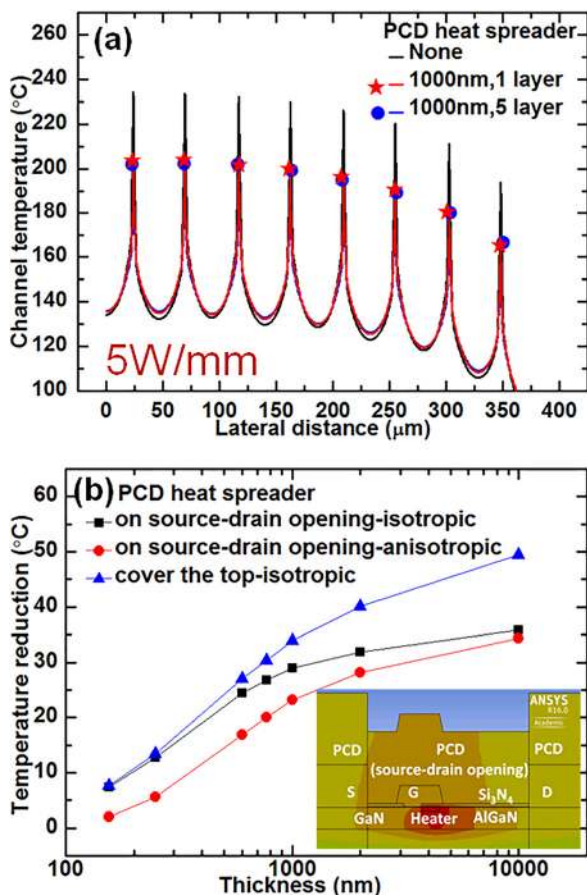
FIG. 4. (a) Peak channel temperature distribution in the lateral direction with and without the 1000 nm PCD film layer. (b) Device peak temperature as a function of the PCD film thickness; the lines are guides to the eye. Inset: schematic of PCD grown on source-drain opening and metal contacts.

[1]U. K. Mishra, L. Shen, T. E. Kazior, and Y.-F. Wu, Proc. IEEE **96**(2), 287–305 (2008).

[2]B. Gelmont, K. Kim, and M. Shur, J. Appl. Phys. **74**(3), 1818–1821 (1993).

[3]R. Gaska, A. Osinsky, J. Yang, and M. S. Shur, IEEE Electron Device Lett. **19**(3), 89–91 (1998).

[4]A. Sarua, H. Ji, M. Kuball, M. J. Uren, T. Martin, K. P. Hilton, and R. S. Balmer, IEEE Trans. Electron Devices **53**(10), 2438–2447 (2006).

[5]R. J. Trew, D. S. Green, and J. B. Shealy, IEEE Microwave Mag. **10**(4), 116–127 (2009).

[6]A. Manoi, J. W. Pomeroy, N. Killat, and M. Kuball, IEEE Electron Device Lett. **31**(12), 1395–1397 (2010).

[7]Y. Won, J. Cho, D. Agonafer, M. Asheghi, and K. E. Goodson, paper presented at the Compound Semiconductor Integrated Circuit Symposium (CSICS), 2013 (IEEE, 2013).

[8]J. G. Felbinger, M. Chandra, Y. Sun, L. F. Eastman, J. Wasserbauer, F. Faili, D. Babic, D. Francis, and F. Ejeckam, IEEE Electron Device Lett. **28**(11), 948–950 (2007).

[9]S. Coe and R. Sussmann, Diamond Relat. Mater. **9**(9), 1726–1729 (2000).

[10]D. Dumka, T. Chou, F. Faili, D. Francis, and F. Ejeckam, Electron. Lett. **49**(20), 1298–1299 (2013).

[11]D. Francis, F. Faili, D. Babić, F. Ejeckam, A. Nurmikko, and H. Maris, Diamond Relat. Mater. **19**(2), 229–233 (2010).

[12]V. Goyal, A. V. Sumant, D. Teweldebrhan, and A. A. Balandin, Adv. Funct. Mater. **22**(7), 1525–1530 (2012).

[13]M. Alomari, M. Dipalo, S. Rossi, M.-A. Diforte-Poisson, S. Delage, J.-F. Carlin, N. Grandjean, C. Gaquiere, L. Toth, and B. Pecz, Diamond Relat. Mater. **20**(4), 604–608 (2011).

[14]D. Dumka, T. Chou, J. Jimenez, D. Fanning, D. Francis, F. Faili, F. Ejeckam, M. Bernardoni, J. Pomeroy, and M. Kuball, paper presented at the Compound Semiconductor Integrated Circuit Symposium (CSICS), 2013 (IEEE, 2013).

[15]J. W. Pomeroy, M. Bernardoni, D. Dumka, D. Fanning, and M. Kuball, Appl. Phys. Lett. **104**(8), 083513 (2014).

[16]J. W. Pomeroy, R. B. Simon, H. Sun, D. Francis, F. Faili, D. J. Twitchen, and M. Kuball, IEEE Electron Device Lett. **35**(10), 1007–1009 (2014).

[17]H. Sun, R. B. Simon, J. W. Pomeroy, D. Francis, F. Faili, D. J. Twitchen, and M. Kuball, Appl. Phys. Lett. **106**(11), 111906 (2015).

[18]H. Sun, J. W. Pomeroy, R. B. Simon, D. Francis, F. Faili, D. J. Twitchen, and M. Kuball, IEEE Electron Device Lett. **37**(5), 621–624 (2016).

[19]M. J. Tadjer, T. J. Anderson, K. D. Hobart, T. I. Feygelson, J. D. Caldwell, C. R. Eddy, Jr., F. J. Kub, J. E. Butler, B. Pate, and J. Melngailis, IEEE Electron Device Lett. **33**(1), 23–25 (2012).

[20]A. Wang, M. Tadjer, and F. Calle, Semicond. Sci. Technol. **28**(5), 055010 (2013).

[21]T. J. Anderson, A. D. Koehler, K. D. Hobart, M. J. Tadjer, T. I. Feygelson, J. K. Hite, B. B. Pate, F. J. Kub, and C. R. Eddy, IEEE Electron Device Lett. **34**(11), 1382–1384 (2013).

[22]P. Pobedinskas, G. Degutis, W. Dexters, W. Janssen, S. Janssens, B. Conings, B. Ruttens, J. d'Haen, H.-G. Boyen, and A. Hardy, Appl. Phys. Lett. **102**(20), 201609 (2013).

[23]O. A. Williams, M. Nesladek, M. Daenen, S. Michaelson, A. Hoffman, E. Osawa, K. Haenen, and R. Jackman, Diamond Relat. Mater. **17**(7), 1080–1088 (2008).

[24]H. Abrams, Metallography **4**(1), 59–78 (1971).

[25]D. G. Cahill, Rev. Sci. Instrum. **75**(12), 5119–5122 (2004).

[26]P. Hui and H. Tan, IEEE Trans. Compon. Packag. Manuf. Technol.: Part B **17**(3), 426–434 (1994).

[27]G. Chen and P. Hui, Thin Solid Films **339**(1), 58–67 (1999).

[28]J. Cho, Y. Li, W. E. Hoke, D. H. Altman, M. Asheghi, and K. E. Goodson, Phys. Rev. B **89**(11), 115301 (2014).

[29]C. Glassbrenner and G. A. Slack, Phys. Rev. A **134**(4), A1058 (1964).

[30]W. Liu and A. A. Balandin, J. Appl. Phys. **97**(7), 73710–73710 (2005).

[31]Y. Zhao, C. Zhu, S. Wang, J. Tian, D. Yang, C. Chen, H. Cheng, and P. Hing, J. Appl. Phys. **96**(8), 4563–4568 (2004).

[32]M. Bogner, A. Hofer, G. Benstetter, H. Gruber, and R. Y. Fu, Thin Solid Films **591**, 267–270 (2015).

[33]J. Yang, E. Ziade, and A. J. Schmidt, Rev. Sci. Instrum. **87**(1), 014901 (2016).

[34]J. Hartmann, P. Voigt, and M. Reichling, J. Appl. Phys. **81**(7), 2966–2972 (1997).

[35]Y. S. Touloukian and E. H. Buyco, *Specific Heat: Metallic Elements and Alloys, Thermophysical Properties of Matter, Volume 4* (IFI/Plenum, New York, 1970).

[36]A. C. Victor, J. Chem. Phys. **36**(7), 1903–1911 (1962).

[37]C. Moelle, M. Werner, F. SzuÈcs, D. Wittorf, M. Sellschopp, J. Von Borany, H.-J. Fecht, and C. Johnston, Diamond Relat. Mater. **7**(2), 499–503 (1998).

[38]J. Nipko, C.-K. Loong, C. Balkas, and R. Davis, Appl. Phys. Lett. **73**(1), 34–36 (1998).

[39]A. S. Okhotin, A. S. Pushkarskij, and V. V. Gorbachev, *Thermophysical Properties of Semiconductors* (Atomizdat, USSR, 1972).

[40]J. Anaya, S. Rossi, M. Alomari, E. Kohn, L. Tóth, B. Pécz, K. D. Hobart, T. J. Anderson, T. I. Feygelson, and B. B. Pate, Acta Mater. **103**, 141–152 (2016).

[41]A. A. Balandin, Nat. Mater. **10**(8), 569–581 (2011).

[42]J. Anaya, H. Sun, J. Pomeroy, and M. Kuball, paper presented at the 2016 15th IEEE Intersociety Conference on Thermal and Thermomechanical Phenomena in Electronic Systems (ITherm) (2016).

[43]M. Mohr, L. Daccache, S. Horvat, K. Brühne, T. Jacob, and H.-J. Fecht, Acta Mater. **122**, 92–98 (2017).

[44]J. Kuzmik, S. Bychikhin, D. Pogany, E. Pichonat, O. Lancry, C. Gaquiere, G. Tsiakatouras, G. Deligeorgis, and A. Georgakilas, J. Appl. Phys. **109**(8), 086106 (2011).

[45]J. Cho, Z. Li, E. Bozorg-Grayeli, T. Kodama, D. Francis, F. Ejeckam, F. Faili, M. Asheghi, and K. E. Goodson, IEEE Trans. Compon. Packag. Manuf. Technol. **3**(1), 79–85 (2013).

[46]H. Verhoeven, E. Boettger, A. Flöter, H. Reiss, and R. Zachai, Diamond Relat. Mater. **6**(2), 298–302 (1997).

[47]H. Verhoeven, A. Flöter, H. Reiß, R. Zachai, D. Wittorf, and W. Jäger, Appl. Phys. Lett. **71**(10), 1329–1331 (1997).

[48]D. G. Cahill and R. Pohl, Solid State Commun. **70**(10), 927–930 (1989).

[49]M. Shamsa, W. Liu, A. Balandin, C. Casiraghi, W. Milne, and A. Ferrari, Appl. Phys. Lett. **89**(16), 161921 (2006).

[50]J. W. Pomeroy, M. J. Uren, B. Lambert, and M. Kuball, Microelectron. Reliab. **55**(12), 2505–2510 (2015).

[51]J. Anaya, S. Rossi, M. Alomari, E. Kohn, L. Tóth, B. Pécz, and M. Kuball, Appl. Phys. Lett. **106**(22), 223101 (2015).